I. Preparation of $NbCl_4[Me_2PCH_2CH_2PMe_2]_2$. $NbCl_4$ (3.0 g, 12.78 mmol) was suspended in 200 ml of THF and $Me_2PCH_2CH_2PMe_2$ (3.84 g, 25.59 mmol) was added. The flask was stoppered and magnetically stirred for 48 h in the drybox to give a purple solution. The solution was filtered and the residue was washed until the washings were colorless. The THF was removed by rotary evaporation to give purple crystals which were filtered and washed with ether. The yield was 6.68 g (98%), mp >300 °C. The analytical sample was recrystallized from THF and ether at −40 °C to give large purple crystals. Anal. Calcd for $NbCl_4P_4C_{12}H_{32}$: C, 26.94; H, 6.03; Cl, 26.51; P, 23.16. Found: C, 27.03; H, 6.18; Cl, 26.61; P, 23.75. ESR (toluene): $g = 1.962$; $\langle a_{Nb} \rangle = 150.2$ G; $\langle a_P \rangle = 22.0$ G. Magnetic moment (CH_2Cl_2): $\chi_M = 1575.7 \times 10^{-6}$ emu/mol; $\mu_{eff}^{303} = 1.9\ \mu_B$. Visible spectrum ($CH_2Cl_2$): 550 ($\epsilon$ 31), 686 (ϵ 74), 805 nm (ϵ 48).

J. Preparation of $NbCl_4(Et_2PCH_2CH_2PEt_2)_2$. To a suspension of $NbCl_4(THF)_2$ (2.76 g, 7.27 mmol) in tetrahydrofuran was added $Et_2PCH_2CH_2PEt_2$ (3.0 g, 14.55 mmol). The solution rapidly turned dark blue. After being stirred for 30 min the solution was filtered and pentane was added. The solution was cooled to −40 °C overnight to give dark blue crystals. They were filtered and washed with pentane; yield 3.06 g. Anal. Calcd for $C_{20}H_{48}Cl_4NbP_4$: C, 37.11; H, 7.47. Found: C, 37.56; H, 7.35. Magnetic moment (CH_2Cl_2): $\chi_M^{cor} = 1469.0 \times 10^{-6}$ emu/mol; $\mu_{eff}^{cor} = 1.9\ \mu_B$. Visible spectrum ($CH_2Cl_2$): 555 ($\epsilon$ 43), 700 (ϵ 65), 825 nm (ϵ 38).

Acknowledgment. I am grateful to Professor J. Kochi (University of Indiana) and Dr. P. J. Krusic for recording the ESR spectra and to Drs. G. W. Parshall, F. N. Tebbe, U. Klabunde, and R. A. Schunn for helpful discussions and supplying samples of Cp_2NbCl_2 and $(MeCp)_2TaBr_2$.

Registry No. Cp_2NbMe_2, 54373-66-9; $(MeCp)_2TaMe_2$, 54474-29-2; $NbCl_4(THF)_2$, 61247-57-2; $NbCl_4(PEt_3)_2$, 61202-63-9; $NbCl_4(PMe_3)_2$, 61202-64-0; $NbCl_4[Me_2PCH_2CH_2PMe_2]_2$, 61202-65-1; $NbCl_4(Et_2PCH_2CH_2PEt_2)_2$, 61202-66-2; Cp_2NbCl_2, 12793-14-5; $(MeCp)_2TaBr_2$, 61202-67-3; $TaCl_4$, 13569-72-7; $NbCl_4$, 13569-70-5; $TaCl_5$, 7721-01-9; $NbCl_5$, 10026-12-7.

References and Notes

(1) D. L. Kepert, "The Early Transition Metals", Academic Press, New York, N.Y., 1972.
(2) D. A. Miller and R. D. Bereman, *Coord. Chem. Rev.*, **9**, 107 (1972).
(3) F. W. Seigert and H. J. deLiefde Meijer, *Recl. Trav. Chim. Pays-Bas*, **87**, 1445 (1968).
(4) J. Klaus, *Z. Chem.*, **14**, 364 (1974).
(5) I. H. Elson, J. K. Kochi, U. Klabunde, L. E. Manzer, G. W. Parshall, and F. N. Tebbe, *J. Am. Chem. Soc.*, **96**, 7374 (1974).
(6) D. F. Evans, *J. Chem. Soc.*, 2003 (1959).
(7) H. C. Clark and L. E. Manzer, *Inorg. Chem.*, **12**, 362 (1973).
(8) R. R. Schrock, *J. Am. Chem. Soc.*, **96**, 6796 (1974).
(9) F. N. Tebbe and G. W. Parshall, *J. Am. Chem. Soc.*, **93**, 3793 (1971); L. J. Guggenberger, *Inorg. Chem.*, **12**, 294 (1973).
(10) U. Klabunde, unpublished results. $(MeCp)_2TaBr_2$ was prepared by dissolving $(MeCp_2)TaH_3$ (G. W. Parshall and U. Klabunde, *J. Am. Chem. Soc.*, **94**, 9081 (1972)) in bromobenzene. A rapid reaction occurred and $(MeCp)_2TaBr_2$ precipitated from solution as a greenish brown crystalline solid. It was filtered, washed with ether, and dried.
(11) H. Schafer, C. Groser, and L. Bayer, *Z. Anorg. Allg. Chem.*, **265**, 258 (1951).
(12) R. E. McCarley and B. A. Torp, *Inorg. Chem.*, **2**, 540 (1963).
(13) G. W. A. Fowles, D. J. Tedmarsh, and R. A. Walton, *Inorg. Chem.*, **8**, 631 (1969).
(14) S. M. Horner, F. N. Gollier, and S. Y. Tyree, *J. Less-Common Met.*, **13**, 85 (1967).
(15) M. Allbott, K. Feenan, and G. W. A. Fowles, *J. Less-Common Met.*, **6**, 299 (1964).
(16) R. Gut and W. Perron, *J. Less-Common Met.*, **26**, 369 (1972).
(17) D. L. Kepert and K. R. Trigwell, *Aust. J. Chem.*, **28**, 1245 (1975).
(18) T. J. Pinnavaia, G. Podolsky, and P. W. Codding, *J. Chem. Soc., Chem. Commun.*, 242 (1973).
(19) R. J. H. Clark, D. L. Kepert, J. Lewis, and R. S. Nyholm, *J. Chem. Soc.*, 2865 (1965).
(20) R. L. Deutscher and D. L. Kepert, *Inorg. Chem.*, **9**, 2305 (1970).

Contribution from the Department of Chemistry, University of Virginia, Charlottesville, Virginia 22901

Optical Activity of the $^4A_2 \rightleftarrows {}^2E$ Transitions in $Cr(en)_3^{3+}$

G. L. HILMES, H. G. BRITTAIN, and F. S. RICHARDSON*

Received August 17, 1976 AIC605969

Circular dichroism (CD)/absorption and circularly polarized emission (CPE)/total emission spectra are reported for $Cr(en)_3^{3+}$ in the region of the spin-forbidden $^4A_{2g} \rightleftarrows {}^2E_g$, $^2T_{1g}$ intraconfigurational d–d transitions. All spectra are reported for $(-)_{546}[Cr(en)_3Cl_3]$ dissolved in 2:1 ethylene glycol–water solution at room temperature. The absorption and emission anisotropy factors associated with the $^4A_{2g} \rightleftarrows {}^2E_g$ transitions are found to be of similar magnitude (and of identical sign), indicating similar structures of the $Cr(en)_3^{3+}$ system in the ground ($^4A_{2g}$) and emitting (^2E_g) states. A theoretical model is developed for calculating the optical activity of the $^4A_{2g} \rightarrow {}^2E_g$, $^2T_{1g}$, $^4T_{2g}$, and $^4T_{1g}$ transitions in the trigonal-dihedral (D_3) $Cr(en)_3^{3+}$ complex. This model treats both spin–orbit interactions and noncubic (trigonal) ligand field interactions as perturbations upon the cubic, non-spin–orbit coupled states of a Cr^{3+} ion in an octahedral ligand environment. The experimentally observed chiroptical properties of $Cr(en)_3^{3+}$ are discussed and compared with respect to the theoretically calculated results.

Introduction

Co^{3+} and Cr^{3+} complexes of trigonal-dihedral (D_3) symmetry have played a central role as model systems in both experimental and theoretical investigations of natural optical activity in coordination compounds. In most cases the spin-allowed d–d and near-ultraviolet charge-transfer transitions have been the focus of attention in these investigations. Recently, Kaizaki, Hidaka, and Shimura[1] have reported the circular dichroism (CD) spectra associated with the low-energy spin-forbidden d–d transitions in a series of tris-chelate Cr^{3+} complexes. The CD/absorption intensities of these transitions are considerably weaker (by several orders of magnitude) then those associated with their spin-allowed counterparts. The primary mechanism whereby the spin-forbidden transitions acquire intensity (CD and absorption) is through spin–orbit coupling of the low-lying doublet excited states to nearby quartet excited states. Kaizaki, Hidaka, and Shimura[1] employed this mechanism to give a semiquantitative account of their experimental results.

In the present study we examine in some detail the mechanism for generating optical activity in the low-energy spin-forbidden transitions (d–d) of trigonal-dihedral (D_3) Cr^{3+} complexes. Of special interest is the optical activity associated with the $^4A_2 \rightleftarrows {}^2E$ transition. We present experimental data for both the CD and the circularly polarized emission (CPE) of this transition in $Cr(en)_3^{3+}$ (en = ethylenediamine). $Cr(en)_3^{3+}$ exhibits a relatively weak phosphorescence in aqueous solution at room temperature which is partially circularly

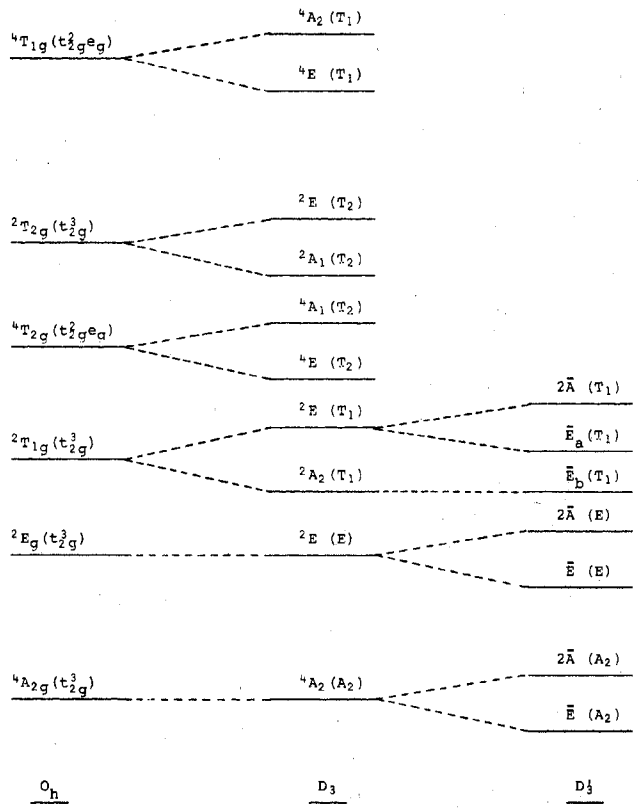

Figure 1. Energy level scheme.

polarized when a resolved (optically active) sample is used.

CPE is the emission analogue of CD and as such provides stereochemical and electronic structural information on molecular emitting states similar to that provided by CD on molecular ground states.[2,3]

Theory

A. General Considerations. A schematic energy level diagram for the states derived from the t_{2g}^3 configuration (quartet and doublet) and from the $t_{2g}^2e_g$ configuration (quartet) is shown in Figure 1. We shall be interested in systems with exact trigonal-dihedral (D_3) symmetry which are six-coordinate through donor atoms which are (nearly) octahedrally disposed about the Cr^{3+} metal ion. Of principal interest are the chiroptical properties associated with the $^4A_2(^4A_{2g}) \rightleftarrows {}^2E(^2E_g)$ transition. Both the $^4A_2(^4A_{2g})$ and $^2E(^2E_g)$ states derive from the t_{2g}^3 3d electron configuration so one may expect that the potential energy curves of these two states are nearly vertically disposed with respect to each other on a configurational-coordinate diagram involving any of the internal (vibrational) nuclear coordinates.

The sign and intensity observables associated with the optical activity of a transition $i \rightarrow j$ may be related to the rotatory strength of this transition

$$R(i \rightarrow j) = \mathrm{Im}\langle\psi_i|\hat{\mu}|\psi_j\rangle\cdot\langle\psi_j|\hat{\mathbf{m}}|\psi_i\rangle \quad (1)$$

where $\hat{\mu}$ and $\hat{\mathbf{m}}$ are respectively the electric and magnetic dipole moment operators and $\mathrm{Im}(a + ib) = b$. Our task, then, is to calculate R for the transition associated with radiative couplings between the $^4A_2(^4A_{2g})$ and $^2E(^2E_g)$ states of our model trigonal-dihedral system.

Our procedure will be to assume that the trigonal-dihedral components of the ligand field potential and the spin–orbit coupling energies are small compared to the octahedral (O_h) components of the ligand field. Given this assumption, the electronic states of the system are described to zeroth order as eigenstates of a Hamiltonian with exact O_h symmetry. The effects of spin–orbit interactions and the trigonal components of the ligand field are then treated by perturbation techniques. Our zeroth-order basis set of interacting states consists of $^4A_{2g}$, ^2E_g, $^2T_{1g}$, $^4T_{2g}$, $^4T_{1g}$, and a $^4T_{2u}$ state. The $^4T_{2u}$ state must be included to generate an electric dipole transition component in the rotatory strength expression (see eq 1). The orbital nature of this ungerade state is left unspecified, although it is assumed that it derives from either a ligand–metal charge-transfer excitation or a 3d → 4p metal excitation.

B. Hamiltonian. The Hamiltonian operator for our model system may be partitioned as follows

$$H = H_0 + V_g + V_u + H_{so} \quad (2)$$

where H_0 is the complete electronic Hamiltonian (excluding spin–orbit interactions) for the zeroth-order (octahedral) representation of the model system, V_g is the component of the trigonal (D_3) ligand field potential which transforms gerade under the inversion operator, V_u is the component of the trigonal (D_3) ligand field potential which transforms ungerade under the inversion operator, and H_{so} is the spin–orbit coupling operator. The zeroth-order wave functions in our model are taken as eigenstates of H_0, and the operators V_g, V_u, and H_{so} are treated as perturbation operators upon these eigenstates.

C. Perturbation Calculation. The influence of $H' = H - H_0$ upon the zeroth-order "octahedral" representation of the system is treated to "all-orders" in perturbation theory by using a variational procedure to obtain the (approximate) eigenstates of $H = H_0 + H'$. In this procedure the Hamiltonian, $H = H_0 + H'$, is diagonalized in a basis consisting of 50 eigenstates (the spin–orbital components of $^4A_{2g}$, ^2E_g, $^2T_{1g}$, $^4T_{2g}$, $^4T_{1g}$, and $^4T_{2u}$) of H_0. The eigenvalues and eigenvectors obtained from this diagonalization are then used to determine the approximate eigenenergies and wave functions of the trigonal-field and spin–orbit "perturbed" model system. The input parameters for this diagonalization calculation are (1) the zeroth-order energies of the basis states, (2) the spin–orbit interaction matrix elements, and (3) the trigonal-field (V_g and V_u) interaction matrix elements.

D. Rotatory Strengths. Denoting the zeroth-order basis functions by $\{\chi_\alpha\}$, we may express the perturbed wave functions of our trigonal model system as

$$\psi_i = \sum_{\alpha=1}^{50} c_{i\alpha}\chi_\alpha \quad (3)$$

where the coefficients $\{c_{i\alpha}\}$ are just the eigenvectors obtained by diagonalization of the $\tilde{\mathbf{H}}$ matrix. The rotatory strength associated with the $i \rightarrow j$ transition may now be written as

$$R(i \rightarrow j) = \mathrm{Im}[\sum_{\alpha}\sum_{\beta}\sum_{\gamma}\sum_{\epsilon} c^*_{i\alpha}c_{j\beta}c^*_{j\gamma}c_{i\epsilon}\langle\chi_\alpha|\hat{\mu}|\chi_\beta\rangle\cdot\langle\chi_\gamma|\hat{\mathbf{m}}|\chi_\epsilon\rangle] \quad (4)$$

To calculate $R(i \rightarrow j)$, the coefficient matrices $\tilde{\mathbf{c}}_i$ and $\tilde{\mathbf{c}}_j$ are required along with the electric dipole and magnetic dipole transition matrices, $\tilde{\boldsymbol{\mu}}$ and $\tilde{\mathbf{m}}$, respectively. The coefficient matrices are obtained from the diagonalization of $\tilde{\mathbf{H}}$.

In the actual calculations performed in this study we neglect perturbations on the $^4A_{2g}$ ground state since these will have little effect upon the chiroptical properties associated with the $^4A_2(^4A_{2g}) \rightleftarrows {}^2E(^2E_g)$ transitions. Zero-field splittings within $^4A_{2g}$ and mixings of $^4A_{2g}$ with excited states are too small to lead to observable features in the fluid-phase optical spectra of the trigonal systems of interest here. This neglect of perturbation upon $^4A_{2g}$ drastically simplifies the construction of the relevant electric dipole and magnetic dipole transition matrices. For the electric dipole transition matrix we need to consider only those elements connecting the four spin–orbital components of $^4A_{2g}$ ($|^4A_{2g}, {}^3/_2\rangle$, $|^4A_{2g}, {}^1/_2\rangle$, $|^4A_{2g}, {}^{-1}/_2\rangle$, and $|^4A_{2g}, {}^{-3}/_2\rangle$) with the 12 spin–orbital components of $^4T_{2u}$. This 4×12 matrix is shown in Table I. For the magnetic dipole transition matrix we need consider only those elements

Table I. Electric Dipole Transition Matrix for $^4A_{2g}$ and $^4T_{2u}$ States, $\langle\mu\rangle$[a]

	$\|^4A_{2g}, {}^3/_2\rangle$	$\|^4A_{2g}, {}^1/_2\rangle$	$\|^4A_{2g}, -{}^1/_2\rangle$	$\|^4A_{2g}, -{}^3/_2\rangle$
$\langle^4T_{2u}X_+, {}^3/_2\|$	k^-	0	0	0
$\langle^4T_{2u}X_+, {}^1/_2\|$	0	k^-	0	0
$\langle^4T_{2u}X_+, -{}^1/_2\|$	0	0	k^-	0
$\langle^4T_{2u}X_+, -{}^3/_2\|$	0	0	0	k^-
$\langle^4T_{2u}X_0, {}^3/_2\|$	$-k^0$	0	0	0
$\langle^4T_{2u}X_0, {}^1/_2\|$	0	$-k^0$	0	0
$\langle^4T_{2u}X_0, -{}^1/_2\|$	0	0	$-k^0$	0
$\langle^4T_{2u}X_0, -{}^3/_2\|$	0	0	0	$-k^0$
$\langle^4T_{2u}X_-, {}^3/_2\|$	k^+	0	0	0
$\langle^4T_{2u}X_-, {}^1/_2\|$	0	k^+	0	0
$\langle^4T_{2u}X_-, -{}^1/_2\|$	0	0	k^+	0
$\langle^4T_{2u}X_-, -{}^3/_2\|$	0	0	0	k^+

[a] In units of $(1/3)^{1/2}\langle^4T_{2u}\|\mu\|^4A_{2g}\rangle = P_r$.

Table II. Magnetic Dipole Transition Matrix for $^4A_{2g}$ and $^4T_{2g}$ States, $\langle m\rangle$[a]

	$\|^4A_{2g}, {}^3/_2\rangle$	$\|^4A_{2g}, {}^1/_2\rangle$	$\|^4A_{2g}, -{}^1/_2\rangle$	$\|^4A_{2g}, -{}^3/_2\rangle$
$\langle^4T_{2g}X_+, {}^3/_2\|$	k^-	0	0	0
$\langle^4T_{2g}X_+, {}^1/_2\|$	0	k^-	0	0
$\langle^4T_{2g}X_+, -{}^1/_2\|$	0	0	k^-	0
$\langle^4T_{2g}X_+, -{}^3/_2\|$	0	0	0	k^-
$\langle^4T_{2g}X_0, {}^3/_2\|$	$-k^0$	0	0	0
$\langle^4T_{2g}X_0, {}^1/_2\|$	0	$-k^0$	0	0
$\langle^4T_{2g}X_0, -{}^1/_2\|$	0	0	$-k^0$	0
$\langle^4T_{2g}X_0, -{}^3/_2\|$	0	0	0	$-k^0$
$\langle^4T_{2g}X_-, {}^3/_2\|$	k^+	0	0	0
$\langle^4T_{2g}X_-, {}^1/_2\|$	0	k^+	0	0
$\langle^4T_{2g}X_-, -{}^1/_2\|$	0	0	k^+	0
$\langle^4T_{2g}X_-, -{}^3/_2\|$	0	0	0	k^+

[a] In units of $2i\,\mu_B$.

connecting the four spin–orbital components of $^4A_{2g}$ with the twelve spin–orbital components of $^4T_{2g}$. This 4 × 12 matrix is shown in Table II.

Given the coefficient matrices, $\tilde{c}_i$ and $\tilde{c}_j$, and the electric dipole and magnetic dipole transition matrices of Tables I and II, the rotatory strengths of the i → j transitions (where i = components of $^4A_{2g}$) may be calculated directly.

CD/Absorption and CPE/Emission Results

The CD/absorption spectra of resolved $[Cr(en)_3(ClO_4)_3]$ in aqueous solution have been reported previously within the region of the spin-forbidden $^4A_{2g} \rightarrow {}^2E_g$, $^2T_{1g}$ transitions.[1] In the present study, we report the CD/absorption spectra of resolved $[Cr(en)_3Cl_3]$ in 2:1 ethylene glycol–water solution at room temperature. These spectra are presented in Figure 2 for the $^4A_{2g} \rightarrow {}^2E_g$, $^2T_{1g}$ transition region.

The CD/total emission spectra of resolved $[Cr(en)_3Cl_3]$ in 2:1 ethylene glycol–water solution are also shown in Figure 2. CPE intensities are reported in arbitrary units of $\Delta I = I_L - I_R$ (where I_L and I_R refer, respectively, to the intensities of the left and right circularly polarized components of the emission), and total emission is reported in arbitrary units of $I = I_L + I_R$. Neither ΔI nor I were measured in absolute intensity units. However, the absolute values of the ratio $g_{em} = \Delta I/(I/2)$ were measured. We shall refer to g_{em} as the emission anisotropy factor, which is analogous to the absorption anisotropy factor, $g_{abs} = \Delta\epsilon/\epsilon$, which may be determined from CD/absorption measurements.[2,3] In general, both g_{em} and g_{abs} are frequency dependent and should be expressed as functions of frequency (or wavelength).

The CD spectrum of $[Cr(en)_3Cl_3]$ shows three clearly resolved components in the region of the $^4A_{2g} \rightarrow {}^2E_g$, $^2T_{1g}$ spin-forbidden transitions. Kaizaki, Hidaka, and Shimura[1] also observed the same CD pattern in this spectral region for $[Cr(en)_3(ClO_4)_3]$ in water. They assigned the low-frequency CD band to the $^4A_{2g} \rightarrow {}^2E_g$ transition and the two higher frequency CD bands to trigonal components of the $^4A_{2g} \rightarrow {}^2T_{1g}$ transition. The absorption spectrum of $[Cr(en)_3Cl_3]$ in this spectral region also shows three features which may be matched up with individual CD extrema if allowance is made for a slight blueshift in frequency in going from the absorption maxima to the corresponding CD extrema. The g_{abs} values associated with the three CD extrema are closely similar.

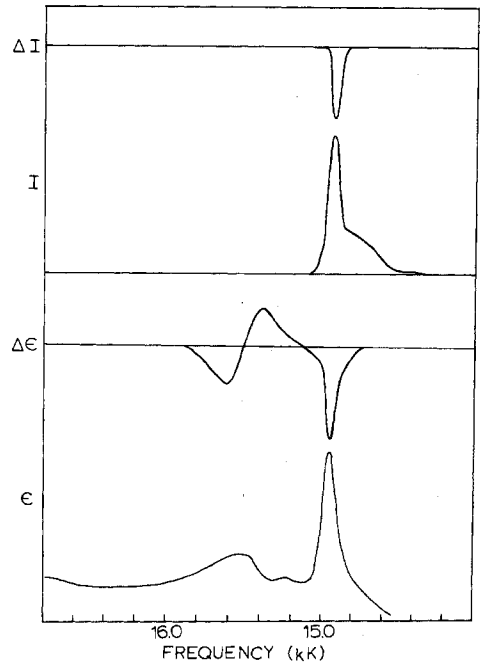

Figure 2. Absorption (ϵ), circular dichroism ($\Delta\epsilon$), total emission (I), and circularly polarized emission (ΔI) spectra for $(-)_{546}[Cr(en)_3Cl_3]$ in a 2:1 ethylene glycol–water solution at room temperature.

Table III. Summary of Experimental Data for $(-)_{546}[Cr(en)_3Cl_3]$ in a 2:1 Ethylene Glycol–Water Solution at Room Temperature

CD/absorption					CPE/emission	
$10^{-3}\bar{\nu}$, cm^{-1}	ϵ	$10^{-3}\bar{\nu}$, cm^{-1}	$\Delta\epsilon$	g_{abs}	$10^{-3}\bar{\nu}$, cm^{-1}	g_{em}
14.95	0.52	14.95	−0.016	−0.031	14.9	−0.046
15.25	0.15	15.4	0.007	0.040		
15.55	0.22	15.6	−0.007	−0.032		
21.75	76.8	21.80	−1.44	−0.019		

The room-temperature phosphorescence of $[Cr(en)_3Cl_3]$ in 2:1 ethylene glycol–water solution exhibits a maximum at 14 901 cm^{-1} and a CPE extremum at exactly the same frequency. The (total) emission band is slightly asymmetric about this frequency, showing a slower falloff in intensity on the low-frequency side. This asymmetry is less pronounced in the 77 K phosphorescence spectrum, but it increases as a function of irradiation time at both room temperature and 77 K. After long periods of irradiation (~1 h at 458 nm), prominent shoulders appear on both the low-frequency and high-frequency sides of the 14 901-cm^{-1} emission band suggesting the formation of photodegradation products.

Additional evidence for the occurrence of photodegradation and/or photoracemization is the reduction in CPE intensity (at 14 901 cm^{-1}) as a function of irradiation time. Irradiation at 458 nm for ~1 hr (using an argon ion laser source) leads to an approximately 50% reduction in CPE intensity. Photoracemization would lead to a reduction in CPE intensity; however, it would not be expected to alter the total emission spectrum. Significant alterations in the total emission spectrum accompanied by a reduction of CPE intensity suggests formation of achiral or racemic photoproducts which are structurally different from the tris complex. The spectra

shown in Figure 2 and the data summarized in Table III were obtained on freshly prepared samples, and the emission experiments were conducted within a period of ~15 min (CPE and total emission are measured and recorded simultaneously). The 14 901-cm^{-1} emission is assigned to the $^4A_{2g} \leftarrow {}^2E_g$ transition.

The near coincidence (in frequency) of the CPE extremum and the first CD band suggest nearly identical geometries for the ground and emitting states of the intraconfigurational $^4A_{2g} \rightleftarrows {}^2E_g$ d–d transitions. However, the larger g_{em} vs. g_{abs} value for these transitions indicates that the emitting state senses a slightly greater chirality (dissymmetry) in the ligand environment.

Calculations

The model outlined in the Theory presumes that the $^4A_{2g} \rightarrow {}^2E_g$, $^2T_{1g}$ transitions in $Cr(en)_3^{3+}$ acquire rotatory strength through the combined perturbative influence of spin–orbit couplings and trigonal (D_3) field interactions among the $^4A_{2g}$, ^2E_g, $^2T_{1g}$, $^4T_{2g}$, $^4T_{2g}$, and $^4T_{2u}$ zeroth-order (octahedral) states of the system. To perform calculations on this model requires knowledge of the reduced matrix elements associated with the electric and magnetic dipole transition integrals, the spin–orbit interactions, and the trigonal field interactions.

A. Electric Dipole Transition Integrals. Choosing z as the trigonal (C_3) axis of our model system, we define the electric dipole operator as

$$\hat{\mu} = -\mu_- \mathbf{k}^+ - \hat{\mu}_+ \mathbf{k}^- + \hat{\mu}_0 \mathbf{k}^0 \tag{5}$$

where

$$\hat{\mu}_+ = -(1/2)^{1/2}(\mu_x + i\mu_y) = -er(4\pi/3)^{1/2} Y_{11}(\theta,\phi) \tag{6}$$

$$\hat{\mu}_- = (1/2)^{1/2}(\hat{\mu}_x - i\mu_y) = -er(4\pi/3)^{1/2} Y_{1-1}(\theta,\phi) \tag{7}$$

$$\hat{\mu}_0 = \hat{\mu}_z = -er(4\pi/3)^{1/2} Y_{10}(\theta,\phi) \tag{8}$$

and

$$\hat{\mathbf{k}}^+ = -(1/2)^{1/2}(\mathbf{i} + i\,\hat{\mathbf{j}}) \tag{9}$$

$$\hat{\mathbf{k}}^- = (1/2)^{1/2}(\mathbf{i} - i\hat{\mathbf{j}}) \tag{10}$$

$$\hat{\mathbf{k}}^0 = \hat{\mathbf{k}} \tag{11}$$

In eq 9–11, $\hat{\mathbf{i}}$, $\hat{\mathbf{j}}$, and $\hat{\mathbf{k}}$ are unit vectors in the directions of the x, y, and z coordinate axes, respectively. In eq 6–8, e is the electron charge and r, θ, and ϕ are the (chromophoric) electron coordinates in spherical polar form. The relevant electric dipole transition integrals may all be calculated to within a radial factor, P_r, by application of coupling tables and symmetry rules.[4,5] The specification of P_r depends, of course, upon the detailed nature of the wave functions appropriate to the states of the system. In the present study, P_r is treated as a variable parameter.

B. Magnetic Dipole Transition Integrals. The magnetic dipole operator, $\hat{\mathbf{m}}$, is defined as

$$\hat{\mathbf{m}} = -\hat{m}_- \hat{\mathbf{k}}^+ - \hat{m}_+ \hat{\mathbf{k}}^- + \hat{m}_0 \hat{\mathbf{k}}^0 \tag{12}$$

where

$$\hat{m}_+ = (e/2mc)(1/2)^{1/2}(\hat{l}_x + i\hat{l}_y) \tag{13}$$

$$\hat{m}_- = -(e/2mc)(1/2)^{1/2}(\hat{l}_x - i\hat{l}_y) \tag{14}$$

$$\hat{m}_0 = -(e/2mc)\hat{l}_z \tag{15}$$

and m is the electron mass and $\hat{l}_x$, $\hat{l}_y$, and $\hat{l}_z$ are the x, y, and z components, respectively, of the orbital angular momentum operator $\hat{\mathbf{l}}$. We neglect all spin contributions to the magnetic dipole transition integrals. In the present study, we evaluate all magnetic dipole transition matrix elements in the "one-center" approximation and assume that the gerade wave functions are comprised only of 3d orbitals on the metal ion. Making these approximations, the relevant magnetic dipole transition integrals may be evaluated exactly (parameter free). The necessary $\langle\hat{\mathbf{m}}\rangle$ matrix elements are listed in Table II.

C. Spin–Orbit Interactions. The one-electron spin–orbit interaction operator, H_{so}, may be written as

$$H_{so} = \xi(r)\hat{\mathbf{l}}\cdot\hat{\mathbf{s}} \tag{16}$$

In evaluating the matrix elements of H_{so} within the basis set of states defined for our model, we again neglect all multicentered terms and assume that the wave functions are comprised of pure metal (ion) orbitals. The $\hat{\mathbf{l}}\cdot\hat{\mathbf{s}}$ parts of the matrix elements are then easily calculated by use of appropriate coupling tables and symmetry rules (for the D_3' double group).[4,5] The radial-dependent parts of the matrix elements, however, are parameterized in terms of the spin–orbit coupling parameter ζ

$$\zeta = \int_0^\infty dr\, r^2 R_d^2(r)\xi(r) \tag{17}$$

where $R_d(r)$ is the radial part of the metal ion 3d orbital.

D. Trigonal Field Interactions. The noncubic (D_3) parts of the ligand field in our model are broken down into components which transform gerade (V_g) under the inversion operation and components which transform ungerade (V_u) under inversion. The gerade part may be expressed as

$$V_g = (1/3)^{1/2}[V_\xi(T_{2g}) + V_\eta(T_{2g}) + V_\zeta(T_{2g})] \tag{18}$$

and the ungerade part may be expressed as

$$V_u = (1/3)^{1/2}[V_\xi(T_{2u}) + V_\eta(T_{2u}) + V_\zeta(T_{2u})] \tag{19}$$

The interaction matrix elements for V_g and V_u may be readily worked out by use of coupling tables and symmetry rules and expressed in terms of a set of parameters which reflect the detailed nature of the interactions and the radial details of the relevant wave functions.

In the present study, we adopt a four-parameter trigonal field interaction model in which the interaction matrix elements are expressed in terms of

$$K_1 = \langle {}^2T_{1g}||V_g||{}^2T_{1g}\rangle = \langle {}^2T_{1g}||V_g||{}^2E_g\rangle \tag{20}$$

$$K_2 = \langle {}^4T_{2g}||V_g||{}^4T_{2g}\rangle = \langle {}^4T_{1g}||V_g||{}^4T_{1g}\rangle = \langle {}^4A_{2g}||V_g||{}^4T_{1g}\rangle = \langle {}^4T_{2g}||V_g||{}^4T_{1g}\rangle \tag{21}$$

$$K_3 = \langle {}^4T_{2u}||V_g||{}^4T_{2u}\rangle \tag{22}$$

$$K_4 = \langle {}^4T_{2g}||V_u||{}^4T_{2u}\rangle = \langle {}^4T_{1g}||V_u||{}^4T_{2u}\rangle \tag{23}$$

This simple four-parameter model is obviously very approximate, but it retains the essential qualitative features of the problem. We do not attempt to calculate K_1, K_2, K_3, and K_4 a priori, but rather we treat these quantities as variable parameters. K_1, K_2, and K_3 will determine the trigonal field induced splittings of the zeroth-order $^2T_{1g}$, $^4T_{2g}$, $^4T_{1g}$, and $^4T_{2u}$ states, and K_4 will determine the signs and, in part, the magnitudes of the calculated rotatory strengths.

E. Rotatory Strengths. The rotatory strengths of the $^4A_{2g} \rightarrow {}^2E_g$, $^2T_{1g}$ transitions are calculated in terms of 11 input parameters: (1) the radial part of the electric dipole transition integrals, P_r; (2) the spin–orbit coupling parameter, ζ; (3) the trigonal field interaction parameters, K_1, K_2, K_3, and K_4; (4) the energies of the unperturbed excited states, $W(^2E_g)$, $W(^2T_{1g})$, $W(^4T_{2g})$, $W(^4T_{1g})$, and $W(^4T_{2u})$.

At 300 K, splitting within the $^4A_2(^4A_{2g})$ ground state is much less than kT and we assume that all of the spin–orbital components of the ground state are equally populated in the

Table IV. Net Values Calculated for Rotatory Strengths[a]

K_4, cm^{-1}	^2E_g(E)	$^2T_{1g}$(E)	$^4T_{2g}$(E)	$^4T_{2g}$(A_1)	$^4T_{1g}$(E)
$K_1 = K_2 = 100$ cm^{-1}, $K_3 = 300$ cm^{-1}, $\zeta = 200$ cm^{-1}					
−1000	−1.44	0.26	2454	−2379	−53.2
−600	−0.39	0.05	1501	−1474	−19.4
−300	−0.19	0.02	753.3	−737.6	−13.5
−200	−0.11	0.02	502.4	−492.6	−7.82
−100	−0.06	0.01	251.8	−246.2	−3.22
$K_1 = K_2 = -100$ cm^{-1}, $K_3 = -300$ cm^{-1}, $\zeta = 200$ cm^{-1}					
−1000	−1.72	0.31	2399	−2491	37.4
−600	−0.43	0.05	1464	−1518	25.3
−300	−0.22	0.02	733.4	−759.4	13.2
−200	−0.14	0.02	489.2	−559.4	9.06
−100	−0.07	0.01	244.6	−279.7	4.51

[a] Calculated in units of 10^{-42} esu^2 cm^2. For a given set of K_1, K_2, K_3, and ζ, changing the sign of K_4 inverts the signs of the rotatory strengths. All rotatory strengths calculated for $^4A_{2g} \rightarrow {}^2T_{1g}(A_2)$ are $<10^{-44}$ esu^2 cm^2 and the signs of the values are all minus.

absence of exciting radiation. The $^2E(^2E_g)$ level is split by spin–orbit coupling into two levels, both of which are doubly degenerate (see Figure 1). The $^2A_2(^2T_{1g})$ level remains unsplit in the presence of spin–orbit coupling, while the $^2E(^2T_{1g})$ level is split into two levels (each of which is doubly degenerate). Assuming pseudodegeneracy within the ground state, the $^4A_{2g} \rightarrow {}^2E_g$, $^2T_{1g}$ transitions may be treated in terms of five component transitions: (1) G → $\bar{E}$(E); (2) G → 2$\bar{A}$(E); (3) G → $\bar{E}_b(T_1)$; (4) G → $\bar{E}_a(T_1)$; (5) G → 2$\bar{A}(T_1)$. G denotes the ground state level (fourfold degenerate) and the remaining symbols are defined as in Figure 1. The energy ordering of these five component transitions is determined by ζ, K_1, K_2, K_3, and $W(^2T_{1g}) - W(^2E_g)$. The relative ordering of the D_3' states in Figure 1 is arbitrary.

F. Parameter Selection. P_r and the zeroth-order state energies were treated as fixed constants in the calculations reported here. The values selected for these parameters are $W(^2E_g) = 15\,000$ cm^{-1}, $W(^2T_{1g}) = 15\,600$ cm^{-1}, $W(^4T_{2g}) = 21\,000$ cm^{-1}, $W(^4T_{1g}) = 26\,500$ cm^{-1}, $W(^4T_{2u}) = 40\,000$ cm^{-1}, and $P_r = 10^{-18}$ esu cm. ζ and the trigonal field parameters (K_1, K_2, K_3, K_4) were treated as calculational variables.

G. Results. The results from representative calculations of rotatory strengths are listed in Tables IV and V for several parameter sets. Only the *net* values associated with transitions to trigonal components of the ^2E_g, $^2T_{1g}$, $^4T_{2g}$, and $^4T_{1g}$ excited states are given.

Discussion

The *net* rotatory strength associated with the $^4A_{2g} \rightarrow {}^4T_{2g}$ transition of $(+)_{546}[Cr(en)_3]^{3+}$ in dilute aqueous solution has been reported as 4.4×10^{-40} esu^2 cm^2 by Karipedes and Piper.[6] The *net* rotatory strength associated with the $^4A_{2g} \rightarrow {}^4T_{1g}$ transition was reported[6] to be -0.72×10^{-40} esu^2 cm^2. Only one CD band is observed in the $^2A_{2g} \rightarrow {}^4T_{2g}$ region for $(+)_{546}[Cr(en)_3]$ in aqueous solution, suggesting either that the trigonal field splitting of the $^4T_{2g}$ state is very small or that the two transitions $^4A_2 \rightarrow {}^4A_1(^4T_{2g})$ and $^4A_2 \rightarrow {}^4E(^4T_{2g})$ have Cotton effects of like signs. Mason[7] has reported a single positive CD band at 458 nm for $2[(+)Cr(en)_3Cl_3]\cdot NaCl\cdot 6H_2O$ doped into the uniaxial crystalline host $2[Rh(en)_3Cl_3]\cdot NaCl\cdot 6H_2O$ and has assigned this CD to the $^4A_2 \rightarrow {}^4E(^4T_{2g})$ transition. The single crystal polarized absorption spectrum of $(+)[Cr(en)_3]^{3+}$ shows the $(\nu_\sigma - \nu_\pi)$ frequency difference to be very small.[6] This latter observation suggests that the $^4E(^4T_{2g})$–$^4A_1(^4T_{2g})$ splitting is also very small, although possibly strong vibronic interactions of the pseudo Jahn–Teller type[8] render such an interpretation ambiguous at best.

Direct molecular orbital calculations[9] on the Λ-lel isomer of $Cr(en)_3^{3+}$ yield a *net* $^4A_{2g} \rightarrow {}^4T_{2g}$ rotatory strength of 1.1 × 10^{-40} esu^2 cm^2 and the following component (trigonal) rotatory strengths: $^4A_2 \rightarrow {}^4E(^4T_{2g})$, 13.5×10^{-40} esu^2 cm^2; $^4A_2 \rightarrow {}^4A_1(^4T_{2g})$, -12.4×10^{-40} esu^2 cm^2. These results were obtained using the dipole length representation in calculating the electric dipole transition integrals. If the dipole velocity representation is used in calculating the electric dipole transition integrals, a *net* rotatory strength of -2.0×10^{-40} esu^2 cm^2 is calculated for the $^4A_{2g} \rightarrow {}^4T_{2g}$ transition and the following component (trigonal) rotatory strengths are obtained:[9] $^4A_2 \rightarrow {}^4E(^4T_{2g})$, 13.1×10^{-40} esu^2 cm^2; $^4A_2 \rightarrow {}^4A_1(^4T_{2g})$, -15.1×10^{-40} esu^2 cm^2. It is unclear, then, from these calculations whether the *net* rotatory strength of the $^4A_{2g} \rightarrow {}^4T_{2g}$ transition should be dominated by the $^4A_2 \rightarrow {}^4E$ component or by the $^4A_2 \rightarrow {}^4A_1$ component.

Table V. Net Values Calculated for Rotatory Strengths[a] ($K_4 = -800$ cm^{-1}, $\zeta = 200$ cm^{-1})

$K_1 = K_2$, cm^{-1}	K_3, cm^{-1}	^2E_g (E)	$^2T_{1g}$ (E)	$^4T_{2g}$ (E)	$^4T_{2g}$ (A_1)	$^4T_{1g}$ (E)
100	100	−0.53	0.08	2007	−1973	−39.0
	−100	−0.53	0.08	2005	−1981	−39.3
	300	−0.52	0.08	2016	−1964	−39.7
	−300	−0.53	0.08	1998	−1993	−39.6
	500	−0.52	0.08	2017	−1953	−39.8
	−500	−0.54	0.08	1993	−2003	−38.9
−100	100	−0.58	0.08	1962	−1986	32.2
	−100	−0.58	0.08	1958	−1995	32.0
	300	−0.58	0.08	1967	−1956	32.1
	−300	−0.59	0.08	1954	−2006	32.0
	500	−0.57	0.08	1973	−1947	32.3
	−500	−0.59	0.08	1949	−2015	31.9
50	100	−0.54	0.08	1988	−1939	−21.9
	−100	−0.55	0.08	1984	−1948	−21.8
	300	−0.54	0.08	1994	−1929	−22.0
	−300	−0.55	0.08	1979	−1958	−21.7
	500	−0.54	0.08	1999	−1920	−22.0
	−500	−0.56	0.08	1973	−1968	−21.5
−50	100	−0.57	0.08	1971	−1953	−13.9
	−100	−0.57	0.08	1968	−1963	−13.9
	300	−0.56	0.08	1976	−1944	−14.0
	−300	−0.57	0.08	1962	−1972	−13.9
	500	−0.56	0.08	1982	−1934	−14.0
	−500	−0.58	0.08	1958	−1998	13.9

[a] Calculated in units of 10^{-42} esu^2 cm^2. For a given set of K_1, K_2, K_3, and ζ, changing the sign of K_4 inverts the signs of the rotatory strengths. All rotatory strengths calculated for $^4A_{2g} \rightarrow {}^2T_{1g}(A_2)$ are $<10^{-44}$ esu^2 cm^2 and the signs of the values are all minus.

According to the calculations performed in the present study, the sign of the *net* rotatory strength associated with the spin-forbidden $^4A_{2g} \rightarrow {}^2E_g$ transition is entirely determined by the sign of K_4 (which originates with the ungerade part of the trigonal field potential). If $K_4 < 0$, then $R_{net}(^4A_{2g} \rightarrow {}^2E_g) < 0$. The sign of $R_{net}(^4A_{2g} \rightarrow {}^2E_g)$ is predicted always to be opposite that of $R(^4A_2 \rightarrow {}^4E(^4T_{2g}))$ and the same as that of $R(^4A_2 \rightarrow {}^4A_1(^4T_{2g}))$. The sign of $R_{net}(^4A_{2g} \rightarrow {}^4T_{2g}) = R(^4A_2 \rightarrow {}^4E) + R(^4A_2 \rightarrow {}^4A_1)$ depends upon the signs and relative magnitudes of K_1, K_2, and K_3 as well as upon the sign and magnitude of K_4. The sign of $R_{net}(^4A_{2g} \rightarrow {}^2E_g)$ is *not* the same as the sign of $R_{net}(^4A_{2g} \rightarrow {}^4T_{2g})$ for all parameter sets examined. This latter result is in contradistinction to the prediction of Kaizaki, Hidaka, and Shimura,[1] who concluded that the signs of $R_{net}(^4A_{2g} \rightarrow {}^4T_{2g})$ and $R_{net}(^4A_{2g} \rightarrow {}^2E_g)$ must be identical.

If the lowest energy Cotton effect in $(-)Cr(en)_3^{3+}$ (near 14 900 cm^{-1}) is assigned to $^4A_{2g} \rightarrow {}^2E_g$ (all components—unresolved in the CD spectra), then $R_{net}(^4A_{2g} \rightarrow {}^2E_g)$ must be negative and $K_4 < 0$. Since it is observed that the *net* CD of the $^4A_{2g} \rightarrow {}^4T_{2g}$ transition is also negative for $(-)Cr(en)_3^{3+}$ in solution, the results given in Tables IV and V suggest that the sign of $R_{net}(^4A_{2g} \rightarrow {}^4T_{2g})$ is determined by the $R(^4A_2 \rightarrow {}^4A_1)$ component. This conclusion is opposite that previously

set forth by Mason and co-workers.[7]

The sign of $R_{net}(^4A_{2g} \rightarrow {}^4T_{1g})$ is calculated to be opposite that of $R_{net}(^4A_{2g} \rightarrow {}^4T_{2g})$ for most (but not all) parameter sets investigated here, a result which is in apparent agreement with experiment.[6] The magnitude and sign of $R_{net}(^4A_{2g} \rightarrow {}^4T_{1g})$ are determined in large part by the sign and magnitude of K_2 since the $^4A_{2g} \rightarrow {}^4T_{1g}$ transition acquires magnitude dipole character via coupling with the $^4A_{2g} \rightarrow {}^4T_{2g}$ transition.

Our calculated values of $R_{net}(^4A_{2g} \rightarrow {}^2E_g)$ are about two orders of magnitude smaller than the calculated values of $R_{net}(^4A_{2g} \rightarrow {}^4T_{2g})$. This result is in approximate agreement with experimental observations. The calculated values of $R_{net}(^4A_{2g} \rightarrow {}^2T_{1g})$ are considerably smaller (by about an order of magnitude) than those of $R_{net}(^4A_{2g} \rightarrow {}^2E_g)$. This latter result is in *qualitative* agreement with experimental observation, although the CD spectra assigned to the $^4A_{2g} \rightarrow {}^2T_{1g}$ transition in Figure 1 cannot be *quantitatively* accounted for by the calculated results. That is, the sign pattern of the CD observed in the $^4A_{2g} \rightarrow {}^2E_g$, $^2T_{1g}$ transition region can be accounted for by assuming a value of $K_4 < 0$; however, the rotatory strengths calculated for components of the $^4A_{2g} \rightarrow {}^2T_{1g}$ transition are somewhat smaller (relative to those calculated for the $^4A_{2g} \rightarrow {}^2E_g$ transition) than can be supported by the experimental data. Our simple six-state model appears to be inadequate with respect to representing accurately the optical activity associated with the $^4A_{2g} \rightarrow {}^2T_{1g}$ transition.

No attempt was made to calculate absorption (or emission) anisotropy values (g_{abs} or g_{em}) in the present study. Recall that, in general, g_{abs} is a function of frequency and is defined by

$$g_{abs}(\nu) = \Delta\epsilon(\nu)/\epsilon(\nu) \tag{24}$$

Integration of $g_{abs}(\nu)$ over the frequency interval spanned by a particular electronic transition, say o $\rightarrow$ n, yields the relationship

$$G_{abs}^{on} = \int_{o\rightarrow n} g_{abs}(\nu)\, d\nu = 4R_{o\rightarrow n}/D_{o\rightarrow n} \tag{25}$$

where $R_{o\rightarrow n}$ and $D_{o\rightarrow n}$ are the rotatory strength and dipole strength, respectively, of the transition o $\rightarrow$ n. For the emissive transition, o′ $\leftarrow$ n′, we may write

$$G_{em}^{o'n'} = \int_{o'\leftarrow n'} g_{em}(\nu)\, d\nu = 4R_{o'\leftarrow n'}/D_{o'\leftarrow n'} \tag{26}$$

where $g_{em}(\nu) = 2\Delta I(\nu)/I(\nu)$ and the integration is performed over the frequency interval spanned by the o′ $\leftarrow$ n′ transition. The wave functions for states o and n are eigenfunctions of the ground state (0) electronic Hamiltonian operator, whereas the wave functions for states o′ and n′ are eigenfunctions of the excited state (n′) electronic Hamiltonian operator. If the molecular (electronic) Hamiltonian for the states o and n′ are identical, then $G_{em}^{o'n'} = G_{abs}^{on}$ for a transition between a given pair of electronic states. Differences between G_{em} and G_{abs} and between g_{abs} and g_{em} indicate structural differences between the ground and excited (emitting) states of the molecular system. The small difference between g_{abs} and g_{em} (observed at $\Delta\epsilon_{max}$ and ΔI_{max}, respectively) for the $^4A_{2g} \rightleftarrows {}^2E_g$ transition (see Table III) suggests slight structural differences between the ground ($^4A_{2g}$) and emitting (^2E_g) states of $Cr(en)_3^{3+}$ in solution. However, the observed difference is very small and barely exceeds the limits of experimental uncertainty. Since this transition involves an intraconfiguration d–d excitation, one would not expect significant structural differences between the ground and (relaxed) excited states.

To calculate $G_{abs}^{on} = 4R_{o\rightarrow n}/D_{o\rightarrow n}$ requires that both the rotatory strength and the dipole strength of the transition be calculated. Since vibronic mechanisms of the Herzberg–Teller variety most certainly will make major contributions to the dipole strengths of transitions in $Cr(en)_3^{3+}$, our model (which excludes vibronic interactions of all kinds) is not adequate for performing calculations of G_{abs}^{on} or of $G_{em}^{o'n'}$.

The major emphasis in this study was upon the mechanism whereby the spin-forbidden $^4A_{2g} \rightarrow {}^2E_g$, $^2T_{1g}$ transitions acquire optical activity in trigonal dihedral $Cr(en)_3^{3+}$. The detailed nature of the trigonal field–chromophoric (3d) electron interactions was not investigated. The trigonal field interaction potential was parameterized (using the parameters K_1, K_2, K_3, and K_4) as were the electric dipole transition integrals (in terms of P_r) and the spin–orbit interaction matrix elements (in terms of ζ). The relative magnitudes and signs of $R_{net}(^4A_{2g} \rightarrow {}^4T_{2g})$ and $R_{net}(^4A_{2g} \rightarrow {}^2E_g)$ were calculated to be in approximate agreement with experimental observation only for trigonal parameter sets which resulted in $|R(^4A_2 \rightarrow {}^4A_1(^4T_{2g}))| > |R(^4A_2 \rightarrow {}^4E(^4T_{2g}))|$. The correct sign for $R_{net}(^4A_{2g} \rightarrow {}^2E_g)$ was calculated only for $K_4 < 0$ values. $R_{net}(^4A_{2g} \rightarrow {}^2T_{1g})$ was calculated to be much smaller than $R_{net}(^4A_{2g} \rightarrow {}^2E_g)$ for all parameter sets examined in this study.

The most obvious refinements of the theoretical model employed in this study should include explicit consideration of vibronic interactions (of the Jahn–Teller, pseudo Jahn–Teller, and Herzberg–Teller types), inclusion of additional spin-doublet states in the basis set, and a more detailed consideration of ungerade states which may mix with the gerade (d–d) states (and provide electric dipole intensity).

Experimental Section

$[Cr(en)_3Cl_3]\cdot 3H_2O$ was prepared according to the method of Gillard and Mitchell[10] and was resolved following the procedure of Galsbol.[11] The CPE/emission experiments were carried out on instrumentation constructed in this laboratory.[2] The excitation source was the 458-nm output of an argon ion laser (Coherent Radiation Model CR-5) which was passed through a Spex "Minimate" monochromator to remove unwanted laser plasma lines. Emission was detected at 180° ("head-on") to the exciting beam. A solution filter of K_2CrO_4 was placed in the emission beam to filter out the exciting light and the emission was dispersed with a $^3/_4$-m single-grating Spex monochromator.

CD/absorption measurements were obtained using a modified Durrum-Jasco J-10B CD spectrophotometer and a Cary 14 absorption spectrophotometer.

All measurements were carried out at room temperature on samples of 0.1 M concentration. A 2:1 mixture of ethylene glycol–H_2O was the solvent.

Acknowledgment. This work was supported by grants from the donors of the Petroleum Research Fund, administered by the American Chemical Society, from the National Science Foundation, and from the Camille and Henry Dreyfus Foundation (through a Teacher-Scholar Award to F.R.).

Registry No. $(-)_{546}[Cr(en)_3Cl_3]$, 31125-86-7.

References and Notes

(1) S. Kaizaki, I. Hidaka, and Y. Shimura, *Inorg. Chem.*, **12**, 135, 142 (1973).
(2) C. K. Luk and F. S. Richardson, *J. Am. Chem. Soc.*, **97**, 6666 (1975).
(3) J. Riehl and F. S. Richardson, *J. Chem. Phys.*, **65**, 1011 (1976).
(4) J. S. Griffith, "The Theory of Transition-Metal Ions", Cambridge University Press, London, 1964.
(5) S. Sugano, Y. Tanabe, and H. Kamimura, "Multiplets of Transition-Metal Ions in Crystals", Academic Press, New York, N.Y., 1970.
(6) A. Karipedes and T. S. Piper, *J. Chem. Phys.*, **40**, 674 (1964).
(7) S. F. Mason in "Fundamental Aspects and Recent Developments in Optical Rotatory Dispersion and Circular Dichroism", F. Ciardelli and P. Salvadori, Ed., Heyden & Son, London, 1973, Chapter 3.6.
(8) F. S. Richardson, D. Caliga, G. Hilmes, and J. J. Jenkins, *Mol. Phys.*, **30**, 257 (1975).
(9) R. S. Evans, A. F. Schreiner, and P. J. Hauser, *Inorg. Chem.*, **13**, 2185 (1974).
(10) R. D. Gillard and P. R. Mitchell, *Inorg. Synth.*, **13**, 184 (1972).
(11) F. Galsbol, *Inorg. Synth.*, **12**, 269 (1971).